doi:10.1093/brain/awq314 Brain 2011: 134; 196–209 | 196

BRAIN
A JOURNAL OF NEUROLOGY

SOD1 targeted to the mitochondrial intermembrane space prevents motor neuropathy in the *Sod1* knockout mouse

Lindsey R. Fischer,[1,*] Anissa Igoudjil,[2,*] Jordi Magrané,[2] Yingjie Li,[1] Jason M. Hansen,[3] Giovanni Manfredi[2] and Jonathan D. Glass[1]

1 Department of Neurology, Emory University School of Medicine, Atlanta, GA 30322, USA
2 Department of Neurology and Neuroscience, Weill Medical College of Cornell University, New York, NY 10065, USA
3 Department of Paediatrics, Emory University School of Medicine, Atlanta, GA 30322, USA

*These authors contributed equally to this work.

Correspondence to: Jonathan D. Glass,
Emory Centre for Neurodegenerative Disease,
101 Woodruff Circle,
Suite 6000, Atlanta,
GA 30322, USA
E-mail: jglas03@emory.edu

Motor axon degeneration is a critical but poorly understood event leading to weakness and muscle atrophy in motor neuron diseases. Here, we investigated oxidative stress-mediated axonal degeneration in mice lacking the antioxidant enzyme, Cu,Zn superoxide dismutase (SOD1). We demonstrate a progressive motor axonopathy in these mice and show that *Sod1*$^{-/-}$ primary motor neurons extend short axons *in vitro* with reduced mitochondrial density. *Sod1*$^{-/-}$ neurons also show oxidation of mitochondrial—but not cytosolic—thioredoxin, suggesting that loss of SOD1 causes preferential oxidative stress in mitochondria, a primary source of superoxide in cells. SOD1 is widely regarded as the cytosolic isoform of superoxide dismutase, but is also found in the mitochondrial intermembrane space. The functional significance of SOD1 in the intermembrane space is unknown. We used a transgenic approach to express SOD1 exclusively in the intermembrane space and found that mitochondrial SOD1 is sufficient to prevent biochemical and morphological defects in the *Sod1*$^{-/-}$ model, and to rescue the motor phenotype of these mice when followed to 12 months of age. These results suggest that SOD1 in the mitochondrial intermembrane space is fundamental for motor axon maintenance, and implicate oxidative damage initiated at mitochondrial sites in the pathogenesis of motor axon degeneration.

Keywords: SOD; axon; neuromuscular junction; motor neuron disease; mitochondria
Abbreviations: $O_2^{\cdot -}$ = superoxide; SOD1 = Cu,Zn superoxide dismutase

Introduction

Motor axons are the anatomical and functional link between spinal motor neurons and skeletal muscles. Degeneration of motor axons at the neuromuscular junction is an early feature of motor neuron disease in animal models (reviewed in Fischer and Glass, 2007) and in humans (Bjornskov *et al.*, 1984; Maselli *et al.*, 1993). Moreover, axonal degeneration is sufficient to cause weakness

Received June 27, 2010. Revised August 18, 2010. Accepted September 11, 2010. Advance Access publication November 14, 2010

and muscle atrophy, even in the absence of motor neuron cell death (Gould *et al.*, 2006; Rouaux *et al.*, 2007; Suzuki *et al.*, 2007). Axon degeneration is therefore a key pathologic event and therapeutic target in motor neuron disease, although the pathogenic mechanisms that initiate axon degeneration are poorly understood.

Evidence from Cu,Zn superoxide dismutase (SOD1) knockout mice suggests that this antioxidant enzyme is essential for motor axon maintenance. *Sod1*$^{-/-}$ mice develop normally and lack behavioural deficits up to 6 months of age (Reaume *et al.*, 1996), but ageing *Sod1*$^{-/-}$ mice perform poorly on the Rotarod and exhibit accelerated skeletal muscle atrophy (Muller *et al.*, 2006). Spinal motor neuron and ventral root axon numbers are normal at 17 and 19 months, respectively (Flood *et al.*, 1999; Shefner *et al.*, 1999), but muscle fibre atrophy and fibre-type grouping, suggestive of chronic denervation and reinnervation, are detectable by 6 months (Flood *et al.*, 1999). EMG recordings also show spontaneous activity and progressive loss of motor units (Shefner *et al.*, 1999). Thus, genetic deletion of SOD1 spares motor neurons and proximal axons, but may be detrimental to distal motor axons.

SOD1 is one of three superoxide dismutases in mammalian cells that catalyse the conversion of superoxide ($O_2{\cdot}^-$) to H_2O_2 (McCord and Fridovich, 1969). SOD1 is traditionally considered to be the cytoplasmic isoform, SOD2 the mitochondrial isoform and SOD3 the secreted form (Zelko *et al.*, 2002). However, SOD1 is also found in the mitochondrial intermembrane space (Weisiger and Fridovich, 1973; Sturtz *et al.*, 2001; Iñarrea, 2002; Vijayvergiya *et al.*, 2005). The functional significance of SOD1 in the intermembrane space remains to be defined, although a protective role is likely. Mitochondria isolated from *Sod1*$^{-/-}$ mouse muscle (Muller *et al.*, 2007; Jang *et al.*, 2010) and *Sod1*$^{-/-}$ *Caenorhabditis elegans* (Yanase *et al.*, 2009) exhibit increased generation of reactive oxygen species including $O_2{\cdot}^-$ and H_2O_2. Similarly, antisense knockdown of SOD1 *in vitro* causes preferential oxidation of mitochondrial—not cytosolic—proteins, loss of mitochondrial membrane potential and decreased ATP production (Aquilano *et al.*, 2006). Thus, loss of SOD1 may result in an accumulation of mitochondrial reactive oxygen species, leading to oxidative damage and mitochondrial dysfunction.

Here, we demonstrate that targeted replacement of SOD1 only in the mitochondrial intermembrane space rescues motor axon outgrowth and normalizes the mitochondrial redox state in *Sod1*$^{-/-}$ neurons *in vitro*, and prevents weakness and neuromuscular junction denervation in *Sod1*$^{-/-}$ mice followed up to 12 months of age. These data suggest that mitochondrial oxidative stress is an underlying cause of distal motor axonopathy, and demonstrate that localization of SOD1 in the intermembrane space is sufficient for the survival of motor axons.

Materials and methods

Animals

Sod1$^{-/-}$ mice, generated by Huang and colleagues (1997), were obtained from Marie Csete (Emory University) (Muller *et al.*, 2006). *Sod1*$^{-/-}$ males were crossed with *thy1-YFP16* females (Feng *et al.*, 2000) to obtain *Sod1*$^{+/-}$, *thy1-YFP16* breeders, expressing yellow fluorescent protein (YFP) in all motor axons. Both transgenic lines were in a C57BL/6 background. For ease of description, *thy1-YFP16* is omitted from the genotype and expression should be assumed. Mice were housed in microisolator cages on a 12 h light–dark cycle and given free access to food and water. Genotyping was by standard polymerase chain reaction analysis on tail-snip DNA. YFP status was determined by fluorescent examination of epidermal nerve fibres in ear punch biopsies.

To generate *mitoSOD1* transgenic mice, human SOD1 complementary DNA was inserted in a prion promoter vector (MoPrP.Xho) (Borchelt *et al.*, 1996) at the XhoI site, between PrP exons 2 and 3. The start codon of human SOD1 was removed and substituted by an in-frame DNA linker of 6 nt, containing a BamHI site and coding for Gly–Ser. We then inserted a 561 nt complementary DNA encoding the first 187 amino acids of mouse mitofilin (GenBank accession code: NM_029673) (John *et al.*, 2005) in frame with the 5′-end of the human SOD1 plus linker. The mitofilin complementary DNA was obtained by polymerase chain reaction amplification of a mouse complementary DNA library using primer sequences derived from the mouse genome database.

The plasmid was microinjected into fertilized eggs of B6CBF1 mice. Offspring harbouring the transgene were identified by polymerase chain reaction using the following primers: CCGCTCGAGATGCTGCG GGCGTGTCAG (sense) and CCGCTCGAGTTATTGGGCGATCCCAAT (antisense) to generate a 1027 bp product. Five lines of *mitoSOD1* transgenic mice were identified. Male founders were crossed with B6SJLF1/J females (Jackson).

A two-step mating scheme was used to generate mice expressing only mitoSOD1. *Sod1*$^{-/-}$ males were crossed with *mitoSOD1* females to generate F1 heterozygotes (*mitoSOD1,Sod1*$^{+/-}$). *Sod1*$^{+/-}$ and *mitoSOD1,Sod1*$^{+/-}$ mice were then crossed to generate the target genotype (*mitoSOD1,Sod1*$^{-/-}$) and littermate controls.

Neuromuscular junction morphology

Tibialis anterior muscle was dissected, pinned in mild stretch and immersion fixed for 30 min in 4% paraformaldehyde at room temperature. Fixed muscles were cryoprotected in 30% sucrose/phosphate-buffered saline (48–72 h at 4°C), flash frozen in supercooled isopentane and 35 μm frozen sections were cut longitudinally through the entire muscle. Acetylcholine receptors at the motor endplate were labelled with Alexa Fluor 555-conjugated α-bungarotoxin (Invitrogen), 1:5000 in phosphate-buffered saline (30 min, room temperature). Motor axon terminals were identified by YFP fluorescence. Innervated, intermediate and denervated endplates were defined by complete, partial or absent overlap between nerve terminal and endplate, respectively. All endplates were evaluated in every fourth section. No difference was seen between innervation in male and female mice, therefore the data were pooled.

Mitochondrial isolation from mouse tissues

Tissues (brain and spinal cord) were homogenized in a Dounce homogenizer in MS-EGTA buffer (225 mM mannitol, 75 mM sucrose, 5 mM HEPES, 1 mM EGTA, pH 7.4), and centrifuged at 2000*g* for 5 min (4°C). The supernatant was centrifuged at 15 000*g* for 20 min to generate the cytosolic fraction (supernatant) and crude mitochondrial fraction (pellet). The cytosolic fraction was centrifuged twice (22 000*g* for 20 min) to eliminate membrane contamination. The crude

mitochondrial fraction was resuspended and washed twice in MS-EGTA. To prepare purified mitochondria, the crude mitochondrial pellet was layered onto 9 ml of 23% Percoll in MS-EGTA and centrifuged at 25 000*g* for 11 min. The pellet was resuspended in MS-EGTA and centrifuged three times at 14 000*g* for 14 min. The final purified mitochondrial pellet was resuspended in MS-EGTA at ~10 mg/ml. All reagents were from Sigma.

Western blot analyses

The expression and mitochondrial localization of mitoSOD1 were tested by western blot of crude mitochondria prepared from spinal cord. Proteins in whole homogenates (50 μg), cytosol (20 μg) and mitochondria (20 μg) were separated on a 12% sodium dodecyl sulphate polyacrylamide gel, transferred to polyvinylidene difluoride membranes (BioRad) and immunoblotted with sheep anti-SOD1 (1:5000, Calbiochem), mouse anti-Tim23 (1:5000, Stressgen), goat anti-Akt1 (1:5000, Santa Cruz) or goat anti-Hsp60 (1:5000, Stressgen).

Blue native gel electrophoresis

Spinal cord mitochondrial proteins (50 μg) were separated on a 10–16% gradient blue native gel as previously described (Schagger and von Jagow, 1991). After electrophoresis, proteins were transferred to polyvinylidene difluoride and immunoblotted for SOD1 and core II subunit of complex III (mouse anti-CIII, 1:2500, Molecular Probes). A high molecular weight ladder (Amersham) was used to estimate protein size.

Alkaline extraction of mitochondrial proteins

Alkaline extraction of mitochondrial proteins was performed as described (Vijayvergiya *et al.*, 2005). Briefly, mitochondria (50 μg) were incubated in the presence or absence of 0.1 M Na_2CO_3 (pH 11.5), with or without Triton X-100 (1%), for 30 min at 4°C, then centrifuged at 91 000*g* for 25 min. The pellet was saved. Supernatant proteins were precipitated with ice-cold 12% trichloroacetic acid and centrifuged at 18 000*g* for 15 min, followed by an ice-cold acetone wash. Pellet and precipitated supernatant proteins were analysed by western blot as described above.

Mitoplast preparation

Mitoplasts were prepared as previously described (Acin-Perez *et al.*, 2009). Briefly, purified mitochondria (300 μg) were suspended in MS-EGTA, water (1/10 volume) and digitonin (1 mg digitonin/5 mg mitochondrial protein), and the mixture was incubated on ice for 45 min. KCl (150 mM) was then added, followed by incubation for 2 min on ice and centrifugation at 18 000*g* for 20 min. The mitoplast pellet was resuspended to 0.5 mg/ml in MS-EGTA. The supernatant containing the post-mitoplast fraction was subjected to trichloroacetic acid precipitation as described above.

Proteinase K treatment of mitoplasts

Proteinase K treatment of mitoplasts was performed as previously described (Vijayvergiya *et al.*, 2005). Briefly, mitoplasts (25 μg) were incubated in the presence or absence of proteinase K (20 μg/ml), with or without Triton X-100 (0.1%), for 1 h on ice. Proteolysis was stopped by adding 2 mM phenylmethylsulphonyl fluoride.

SOD1 activity: spectrophotometric assay

SOD1 activity was assessed as previously described (Vives-Bauza *et al.*, 2007) with minor modifications. The assay measures the reduction of acetylated cytochrome *c* by $O_2\cdot^-$ generated by xanthine/xanthine oxidase. All reagents were from Sigma except for xanthine oxidase (Calbiochem). Spinal cord mitochondria (50 μg) and cytosolic fractions (10 μg) were incubated in 1 ml of reaction buffer (50 mM phosphate buffer, pH 7.8, 0.1 mM EDTA, 1 mM NaN_3, 100 mM xanthine, 2 U xanthine oxidase and 25 mM partially acetylated cytochrome *c*). Cytochrome *c* reduction was followed spectrophotometrically at 550 nm, at 25°C for 3 min. The activity of SOD1 (KCN-insensitive) was determined by adding 2 mM KCN, and subtracting residual activity from total SOD activity. One unit of SOD activity was defined as the amount of enzyme required to inhibit the rate of reduction of cytochrome *c* by 50%. Note that in measuring SOD1 activity in mitochondria it is necessary to minimize the interference associated with the interaction of cytochrome *c* with cytochrome *c* oxidase and cytochrome *c* reductases, using partially acetylated cytochrome *c* as described (Azzi *et al.*, 1975; Kuthan *et al.*, 1986). Nevertheless, we found some residual cytochrome *c* reduction in the mitochondria of $Sod1^{-/-}$ samples (Fig. 5E). This can be explained by the fact that the preparation of acetylated cytochrome *c* actually contains up to 40% non-acetylated cytochrome *c*, which can react with mitochondrial oxidases and reductases.

Primary motor neuron culture

Spinal motor neurons were enriched from E12.5 mouse embryos by density centrifugation (Zhang *et al.*, 2006). Spinal cords were isolated, incubated in 0.05% trypsin (Worthington, 37°, 10 min) and dissociated by pipetting up and down in neurobasal medium (Invitrogen) containing 0.1% trypsin inhibitor (Sigma), 100 U/ml DNase (Worthington) and 0.4% bovine serum albumin. Cells were centrifuged through 4% bovine serum albumin (400*g*, 5 min), resuspended and centrifuged through 10% (v/v) Optiprep (Axis Shield, 700*g*, 10 min). The interface was aspirated, centrifuged through a second bovine serum albumin cushion, and resuspended in growth medium consisting of neurobasal with 2% B27 supplement minus antioxidants (Invitrogen), 2% horse serum (Invitrogen), 0.5 mM Glutamax (Invitrogen), BDNF, CNTF, GDNF and NT-3 (10 ng/ml, Peprotech). Cells were plated on coverslips coated with polyornithine (10 μg/ml, Sigma) and Matrigel (1:25, BD Bioscience). By this method, 84.7 ± 4.8% of cells at 24 h were immunoreactive for the motor neuron marker, Hb9 (1:1000, Abcam). Individual spinal cords were kept separate during cell isolation and genotype subsequently determined by polymerase chain reaction.

Axon length was determined by systematic random sampling of cells along a pre-marked grid. Motor neurons were identified morphologically under phase contrast and photographed at ×20 on an Olympus IK51 inverted microscope using an Olympus Qcolor3 digital camera. Axons were manually traced and measured using ImageJ software (http://rsb.info.nih.gov/ij/). In cells with multiple processes, the axon was considered to be the longest process. The average number of neurons analysed in each of four trials was 130 ± 41 ($Sod1^{+/+}$), 158 ± 34 ($Sod1^{+/-}$) and 163 ± 19 ($Sod1^{-/-}$), or 500–600 neurons per group ($n = 4$ was used for statistical analysis).

Mitochondrial density

Mitochondrial density in axons was evaluated using Mitotracker Red CM-H_2XRos (Invitrogen). Dye was added to cells at 250 nM in serum-free medium (30 min, 37°C). Cells were returned to growth medium for 10 min and fixed in pre-warmed 4% paraformaldehyde (15 min, room temperature). Coverslips were inverted onto slides using anti-fade mounting medium (Vectashield + DAPI, Vector Labs), and cells were examined under standard fluorescence microscopy. In some experiments, Mitotracker staining was followed by immunolabelling with an antibody specific for human SOD1 (Sigma, 1:500). Twenty-five neurons per coverslip were selected and photographed at ×40 magnification by unbiased coverslip scanning. Mitochondrial density was evaluated morphologically using ImageJ software. Lengths of individual mitochondria were measured, combined and divided by the length of the axon. At least three replicates per genotype were obtained over the course of multiple motor neuron preparations.

Primary cortical neuron cultures

Primary cortical neurons were isolated from E15.5 mouse embryos. Brains were removed in ice-cold dissecting buffer (2.5 mM HEPES, 4 mM $NaHCO_3$ and 35 mM glucose in Hanks' balanced salt solution) and cortices were dissected free of subcortical structures and meninges and incubated in 0.25% Trypsin/EDTA (Sigma), for 15 min at 37°C. Tissue was dissociated in dissection buffer containing 0.1 mg/ml trypsin inhibitor (Sigma) and 200 U/ml DNase (Worthington). Cells were pelleted by centrifugation at 218*g* for 5 min and resuspended in growth medium consisting of neurobasal (Invitrogen), 5% foetal bovine serum (Atlanta Biologicals), 200 mM GlutaMAX (Invitrogen) and 2% B27 minus antioxidants (Invitrogen). Cells were plated in poly-L-lysine coated six-well plates at a density of 2×10^6 cells/well. Individual brains were kept separate during cell isolation and genotype subsequently determined by polymerase chain reaction on tail-snip DNA.

Thioredoxin redox western analysis

The redox state of thioredoxin-1 (cytosolic) and thioredoxin-2 (mitochondrial) was determined by redox western analysis (Halvey *et al.*, 2005). Primary cortical neurons were washed once with ice-cold phosphate-buffered saline, incubated in 10% trichloroacetic acid at 4°C for 20 min, and removed with a cell scraper. Following centrifugation at 16 000*g* for 2 min, the protein pellet was washed in 100% acetone and resuspended by sonication in derivatization buffer: 17.5 mM AMS (4-acetamide-4′-maleimidylstilbene-2,2′-disulphonic acid) (Invitrogen) in 100 mM Tris, pH 7.6, 1% sodium dodecyl sulphate. Derivatization was allowed to proceed for 1 h at room temperature. Samples were diluted 1:1 in non-reducing sodium dodecyl sulphate sample buffer (Bio-Rad), boiled and separated on two 15% polyacrylamide gels run in parallel. Immunoblotting was carried out by standard methods using goat anti-thioredoxin-1 (1:2500, American Diagnostica, Stamford, CT, USA) or rabbit anti-thioredoxin-2 (1:5000) (Halvey *et al.*, 2005). Secondary antibodies were AlexaFluor-680-conjugated anti-goat or anti-rabbit, respectively (1:7500, Invitrogen). Membrane scanning and band densitometry were performed on an Odyssey infrared imaging system (Li-COR) using Odyssey software. The redox potential E_h (in mV) was calculated using the Nernst equation: $E_h = E_0 + (2.303\ RT/nF) \times \log(ox/red)$, where $E_0 = -256$ mV (thioredoxin-1) or -330 mV (thioredoxin-2). Note that protein levels were not equalized between samples. Only relative changes between reduced and oxidized bands are of quantitative significance.

Confocal imaging

Images were captured on a Zeiss LSM 510 NLO META system, coupled to a Zeiss Axiovert 100M inverted microscope. Neuromuscular junction *z*-stacks were obtained with a Plan-Neofluar ×40 (NA 1.3) oil objective with optical slice thickness of 1 μm. Motor neurons were imaged with a Plan-Neofluar ×20 (NA 0.3) objective or Plan-Neofluar ×100 (NA 1.3) oil objective. *Z*-stacks were compressed and images exported using LSM Image Examiner software (Zeiss).

Statistical analysis

Results are expressed as mean ± SD, and comparisons were made by ANOVA with Tukey *post hoc* analysis ($\alpha = 0.05$), unless otherwise specified, using Prism software (GraphPad).

Results

Loss of SOD1 causes a progressive motor neuropathy

Previous studies of the *Sod1*$^{-/-}$ mouse provide compelling, although indirect, evidence for a motor axonopathy (Flood *et al.*, 1999; Shefner *et al.*, 1999). To facilitate morphological analysis of neuromuscular junctions, we first crossed *Sod1*$^{-/-}$ mice (Muller *et al.*, 2006) with *thy1-YFP16* mice (Feng *et al.*, 2000) to generate mice expressing YFP in all motor axons. Absence of SOD1 protein and enzymatic activity was verified in *Sod1*$^{-/-}$, *thy1-YFP16* offspring by western blot and SOD1 zymography (Supplementary Fig. 1).

We observed progressive hind-limb weakness in *Sod1*$^{-/-}$ mice, evidenced by significant loss of grip strength by 12 months (Fig. 1C). Whereas most *Sod1*$^{+/+}$ *and* *Sod1*$^{+/-}$ mice could remain suspended from a wire grid for at least 300 s, the mean latency to fall for *Sod1*$^{-/-}$ animals was 134 s ($P < 0.001$). *Sod1*$^{-/-}$ mice had obvious difficulty gripping the wire with their hind limbs, and hind limb grip was typically lost first, followed by forelimb grip (Supplementary Videos 1–4).

To determine how loss of SOD1 affects distal motor axons, we examined neuromuscular junction morphology in the tibialis anterior muscle, which undergoes significant (~50%) atrophy in 20-month-old *Sod1*$^{-/-}$ mice (Muller *et al.*, 2006). Neuromuscular junction innervation at 1, 4, 12 and 18 months of age was evaluated by the overlap between YFP-positive motor axon terminals and motor endplates labelled with Alexa Fluor 555-conjugated α-bungarotoxin (Fig. 1A and B). At 1 month, the tibialis anterior muscle was fully innervated in *Sod1*$^{-/-}$ mice. At 4 months, 69.5 ± 6.2% of endplates were innervated in *Sod1*$^{-/-}$ mice, compared to 97.1 ± 0.9% and 99.6 ± 0.3% in *Sod1*$^{+/+}$ and *Sod1*$^{+/-}$ mice, respectively ($P < 0.001$). By 18 months, only 33.9 ± 8.5% of *Sod1*$^{-/-}$ endplates were innervated compared to 92.2 ± 2.8% in *Sod1*$^{+/+}$ mice and 79.9 ± 15.5% in *Sod1*$^{+/-}$ mice ($P < 0.001$). This demonstrates that SOD1 is required for maintenance of motor

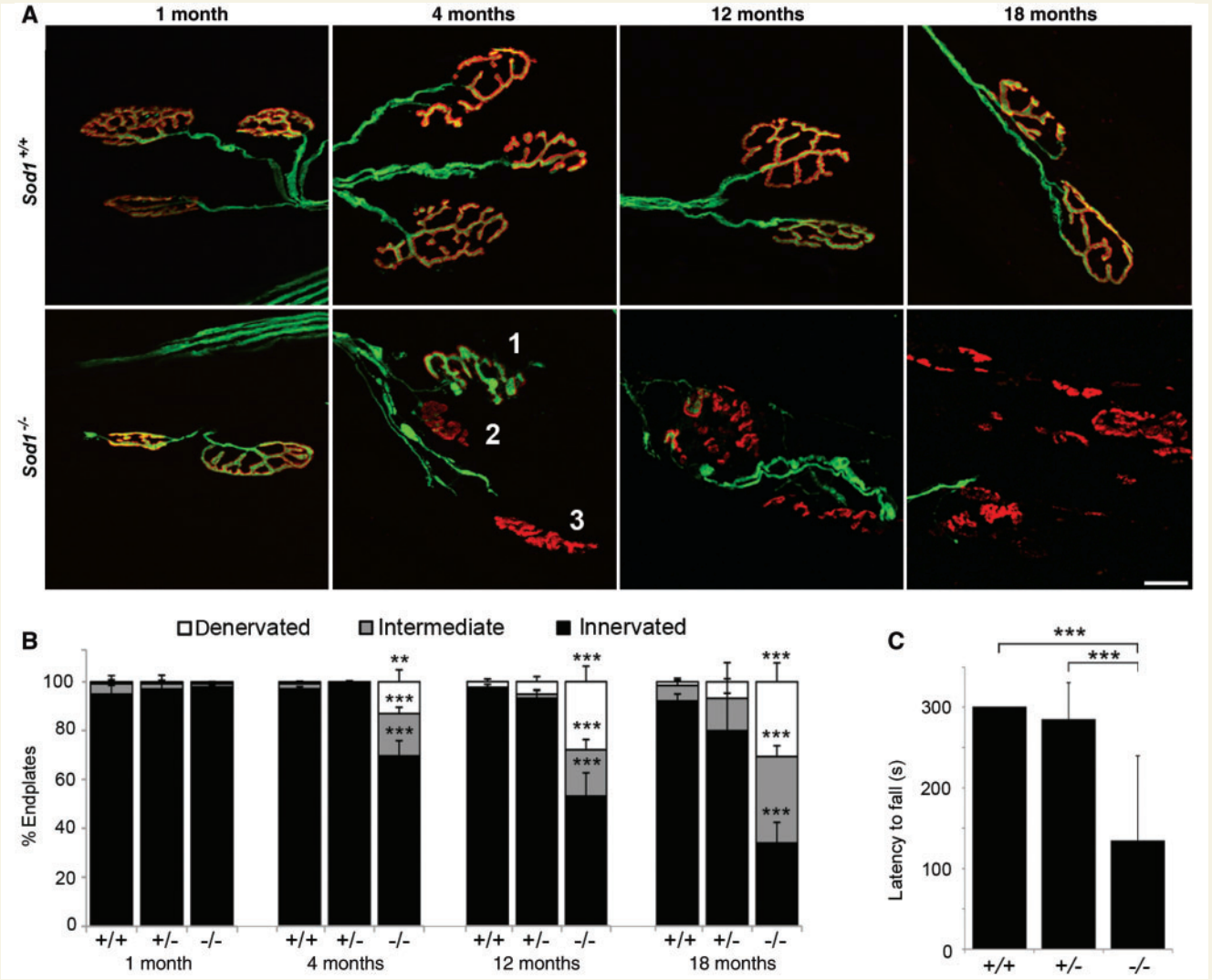

Figure 1 Genetic deletion of SOD1 causes progressive denervation at the neuromuscular junction. (**A**) Confocal projections of tibialis anterior neuromuscular junctions at 1, 4, 12 and 18 months of age, with motor axons in green (yellow fluorescent protein) and endplates in red (bungarotoxin). Examples of innervated (1), intermediate (2) and denervated (3) endplates are shown. By 18 months, many endplates are vacant and show a fragmented morphology consistent with chronic denervation. Fragmentation was not observed in innervated endplates. Scale bar = 20 μm. (**B**) Percent innervated, intermediate and denervated endplates in tibialis anterior. Endplates (898 ± 203) were assessed per muscle. (**$P < 0.01$, ***$P < 0.001$ for $Sod1^{-/-}$ versus $Sod1^{+/+}$; ANOVA with Tukey *post hoc* test; $n = 3$–7 animals per group). (**C**) Latency to fall (s) on grip strength test at 12 months of age. The best performance out of three trials, to a maximum of 300 s, was recorded for each animal (***$P < 0.001$; ANOVA with Tukey *post hoc* test; $n = 6$–9 animals per group).

axons *in vivo,* and suggests that distal motor axons are sensitive to oxidative stress-mediated injury.

Axon defects in primary motor neuron cultures

To examine axonal defects intrinsic to $Sod1^{-/-}$ motor neurons, we cultured primary motor neurons from E12.5 mice in medium free of standard antioxidant supplements (Fig. 2A). $Sod1^{-/-}$ motor neurons were short-lived compared with controls. No viable $Sod1^{-/-}$ cells remained at 72 h in culture. At 24 h, $Sod1^{-/-}$ motor neurons had markedly shorter axons compared with controls (Fig. 2C). Mean axon length in $Sod1^{-/-}$ cells (±SEM) was 50 ± 3 μm at 24 h, compared with 93 ± 5 and 83 ± 3 μm for $Sod1^{+/+}$ and $Sod1^{+/-}$ cells, respectively ($P < 0.001$).

Given a previous report of mitochondrial damage in $Sod1^{-/-}$ cells (Aquilano *et al.*, 2006), we tested whether mitochondrial density was altered in $Sod1^{-/-}$ axons (Fig. 2B). At 24 h in culture, mitochondria were labelled with Mitotracker Red-CM-H_2XRos, the motor neurons were fixed and individual mitochondria along the length of the axon were measured. Mitochondrial density was expressed as the cumulative length of all mitochondria in the axon, divided by the total length of the axon (Fig. 2D).

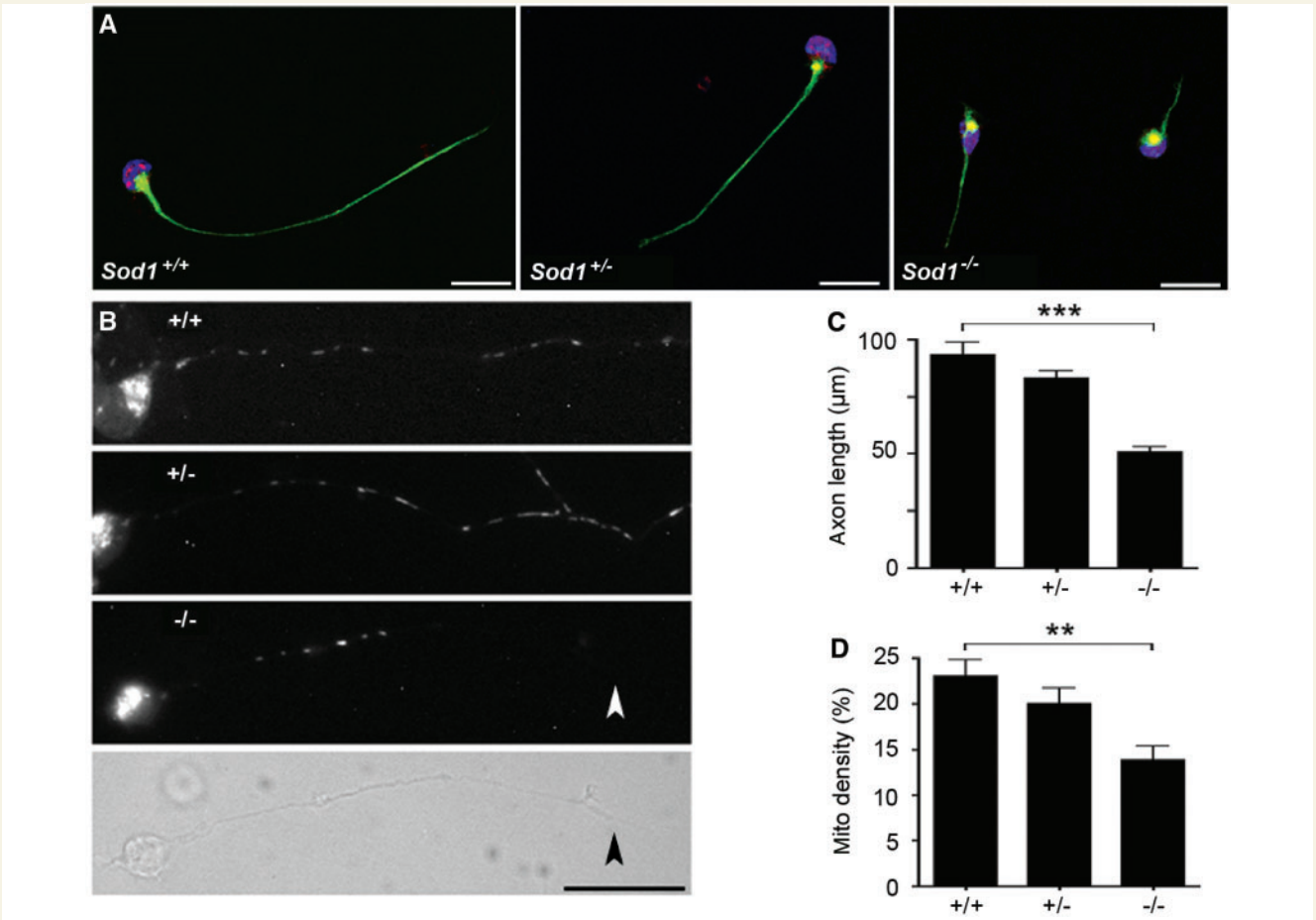

Figure 2 *Sod1*$^{-/-}$ primary motor neurons show reduced axon outgrowth and decreased mitochondrial density. (**A**) *Sod1*$^{+/+}$, *Sod1*$^{+/-}$ and *Sod1*$^{-/-}$ primary motor neurons at 24 h in culture, labelled with phosphorylated neurofilament antibody (NF160, green), Hb9 antibody (red) and DAPI (blue). Scale bar = 20 μm. (**B**) Motor neurons labelled with Mitotracker Red CM-H_2XRos (24 h in culture). A phase contrast image is shown for the *Sod1*$^{-/-}$ motor neuron to visualize the full-length of the axon (the terminal is marked with an arrowhead). Scale bar = 25 μm. (**C**) Axon length at 24 h. The 500–600 neurons per group were measured. Mean ± SEM from $n = 4$ replicates is shown (***$P < 0.001$; ANOVA with Tukey *post hoc* test). (**D**) Mitochondrial density expressed as percentage of axon length occupied by mitochondria. Twenty-five axons per group were analysed. Mean ± SEM from $n = 3$ replicates is shown (**$P < 0.01$; ANOVA with Tukey *post hoc* test).

By this approach, a 40% decrease in mitochondrial density was observed in *Sod1*$^{-/-}$ axons compared to *Sod1*$^{+/+}$ axons ($P < 0.01$).

The mitochondrial redox state in neurons depends on SOD1 expression

We then investigated how deletion of SOD1 in neurons influences the cytosolic versus mitochondrial redox state. To avoid introducing oxidation by subcellular fractionation, we took advantage of the fact that mitochondria have a distinct thioredoxin system from the cytosol, and these can be resolved by using different antibodies on the same sample. Thioredoxins are small, multi-functional proteins with a highly conserved active site dithiol motif (Arnér and Holmgren, 2000). They serve as protein disulphide reductases and participate in reactive oxygen species removal via peroxiredoxins. Redox western analysis of thioredoxin-1 (cytosolic) versus thioredoxin-2 is a sensitive measure of compartmental changes that can occur independent of overall cellular oxidation (Halvey *et al.*, 2005; Hansen *et al.*, 2006*a*, *b*).

Primary cortical neurons were isolated from *Sod1*$^{-/-}$ mice and littermate controls, maintained in culture for 3 days, and harvested for redox western visualization of oxidized and reduced thioredoxin (Fig. 3). *Sod1*$^{+/+}$ neurons showed a thioredoxin-1 redox potential of −273 ± 2 mV and a thioredoxin-2 redox potential of −365 ± 2 mV. These values are consistent with previous data from other cell types, showing that thioredoxin-1 is relatively oxidized at baseline compared with thioredoxin-2 (Halvey *et al.*, 2005; Hansen *et al.*, 2006*a*). The thioredoxin-1 redox potential in *Sod1*$^{-/-}$ neurons (−271 ± 1 mV) was identical to wild-type. However, *Sod1*$^{-/-}$ neurons showed significant oxidation of thioredoxin-2, with a redox potential of −342 ± 7 mV, representing a +23 mV shift toward a more oxidizing potential as compared to controls ($P < 0.01$). This demonstrates oxidative stress occurring

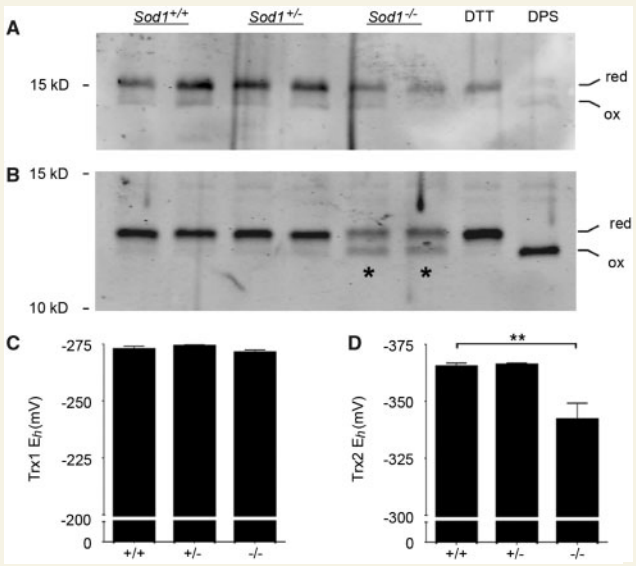

Figure 3 *Sod1*$^{-/-}$ neurons show preferential oxidation of mitochondrial versus cytosolic thioredoxin. (**A**) Thioredoxin-1 (cytosolic) redox western. (**B**) Thioredoxin-2 (mitochondrial) redox western. Asterisks indicate the increased density of the oxidized band in *Sod1*$^{-/-}$ samples. Dithiothreitol (DTT)- and dipyridyldisulfide (DPS)-treated cells were included to verify position of reduced and oxidized bands, respectively. (**C**) Thioredoxin-1 (Trx1) redox potentials (derived using the Nernst equation) show no difference between *Sod1*$^{-/-}$ and controls. (**D**) Thioredoxin-2 (Trx2) shows a +23 mV shift in *Sod1*$^{-/-}$ neurons, toward a more oxidized redox potential. Mean ± SEM is shown for $n = 3$–6 replicates per group (**$P < 0.01$; ANOVA with Tukey *post hoc* test). The *y*-axes are inverted for ease of interpretation.

within mitochondria of *Sod1*$^{-/-}$ neurons, at a time when the cytosolic redox state is unchanged.

Targeting of wild-type human SOD1 to the mitochondrial intermembrane space

To test the hypothesis that SOD1 in the mitochondrial intermembrane space plays a role in motor axon maintenance, transgenic mice were generated that express wild-type human SOD1 targeted to the intermembrane space (Fig. 4A). We fused the N-terminal of SOD1 to the mitochondrial targeting sequence of mouse mitofilin, a mitochondrial inner membrane protein (John *et al.*, 2005). The 34 amino acid mitofilin targeting sequence, cleavable by matrix metalloproteinases, was followed by 153 amino acids of the mature protein, including 26 amino acids of the transmembrane domain and a 2 amino acid linker between mitofilin and the N-terminus of human SOD1. The resulting construct coded for a ~38 kDa chimeric protein (mitoSOD1). This targeting strategy was aimed at anchoring human SOD1 to the outer side of the mitochondrial inner membrane, facing the intermembrane space, while conferring enough flexibility for SOD1 to fold and mature into the active enzyme. Tethering to the inner membrane was designed to prevent unwanted escape of mitoSOD1 into the cytosol. For

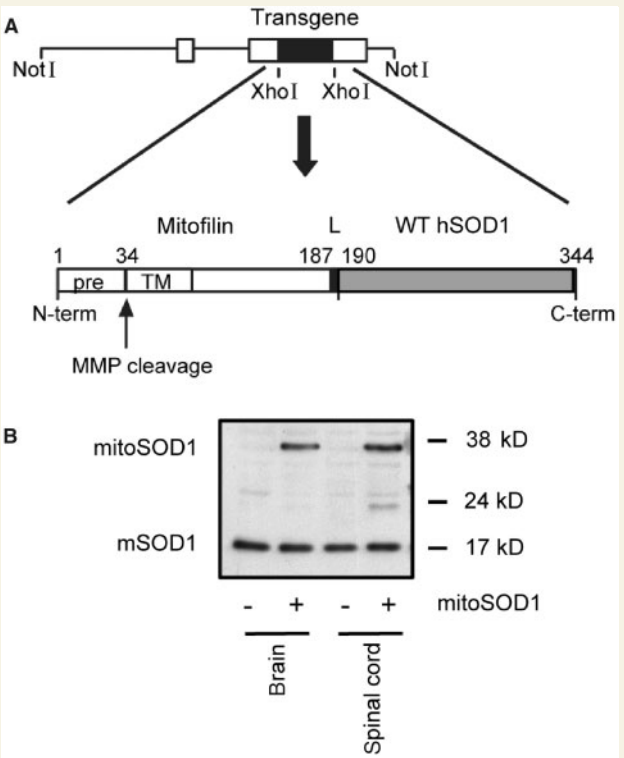

Figure 4 Generation of mice expressing wild-type human SOD1 targeted to the mitochondrial intermembrane space. (**A**) Schematic representation of the strategy to create the *mitoSOD1* transgene cloned in the mouse prion promoter vector. (**B**) Detection of mitoSOD1 in non-transgenic (–) and transgenic (+) mouse tissues by western blot, using a sheep polyclonal SOD1 antibody that recognizes both transgenic human mitoSOD1 and endogenous mouse SOD1 (mSOD1). WT hSOD1 = wild-type human SOD1; pre = mitochondrial targeting presequence; TM = transmembrane domain; L = 2 amino acid linker; MMP = matrix metalloproteinases.

generation of transgenic mice, the construct was cloned downstream of the mouse prion promoter, which drives high expression in brain, spinal cord, skeletal muscle, heart and kidney, low expression in lung and spleen and virtually no expression in liver (Wang *et al.*, 2005).

Five lines of transgenic mice with different levels of expression were obtained. For this study, we utilized the line with the highest level of mitoSOD1 expression. The pattern of mitoSOD1 expression in different tissues was investigated by western blot of whole tissue homogenates (Fig. 4B). The 38 kDa mitoSOD1 protein was expressed in brain and spinal cord of transgenic mice and not in non-transgenic controls (Fig. 4B). MitoSOD1 was also detected in skeletal muscle, heart and kidney, while lung, spleen and liver expressed low to undetectable levels (Supplementary Fig. 2).

Generation and characterization of mice expressing only mitoSOD1

Next we crossed *mitoSOD1* and *Sod1*$^{-/-}$ mice in a two-step breeding process, to generate *mitoSOD1,Sod1*$^{-/-}$ mice expressing SOD1 only in the intermembrane space. Littermate *mitoSOD1,Sod1*$^{+/+}$ and

Sod1$^{+/+}$ mice were used as controls. Fractionation of spinal cord homogenates confirmed that the mitoSOD1 was detected only in the mitochondrial fraction from *mitoSOD1,Sod1*$^{+/+}$ and *mitoSOD1,Sod1*$^{-/-}$ mice, and was undetectable in the cytosol (Fig. 5A). As expected, no mouse SOD1 was detected in the mitochondria or cytosol of *Sod1*$^{-/-}$ and *mitoSOD1, Sod1*$^{-/-}$ spinal cords.

Protein alkaline extraction of brain mitochondria from *mitoSOD1* mice showed the transgenic protein almost exclusively in the insoluble pellet, whereas cytochrome *c*, a soluble protein of the intermembrane space, was found in the supernatant (Fig. 5B). Most of the mitoSOD1 transgenic protein was released in the soluble fraction after treatment of the mitochondrial membranes with Triton X-100. This indicates that mitoSOD1 is anchored to the mitochondrial inner membrane through its transmembrane domain.

To study the intra-mitochondrial localization of mitoSOD1, mitoplasts were prepared by removing the mitochondrial outer membrane from *mitoSOD1,Sod1*$^{+/+}$ brain mitochondria. MitoSOD1 was associated with mitoplasts and absent from the post-mitoplast supernatant containing the outer membrane and intermembrane space fractions (Fig. 5C). Following digestion of mitoplast surface proteins with proteinase K, most of the mitoSOD1 was degraded to a smaller ~19 kDa fragment. This fragment displayed gel migration properties roughly corresponding to those of human SOD1, which is proteinase K resistant (Vijayvergiya *et al*., 2005), indicating that proteinase K digested the portion of the protein anchoring SOD1 to the inner membrane. This result was reproduced by solubilization of mitoplasts with Triton X-100 followed by proteinase K digestion. Taken together, these results confirm that mitoSOD1 is bound to the mitochondrial inner membrane facing the intermembrane space.

MitoSOD1 enzyme activity was assessed in whole spinal cord lysates by standard SOD1 zymography (Supplementary Fig. 3). An additional band of KCN-sensitive SOD1 activity was identified in *mitoSOD1,Sod1*$^{+/+}$ and *mitoSOD1,Sod1*$^{-/-}$ mice, demonstrating that mitoSOD1 protein is enzymatically active. To address subcellular localization and avoid disruption of mitoSOD1

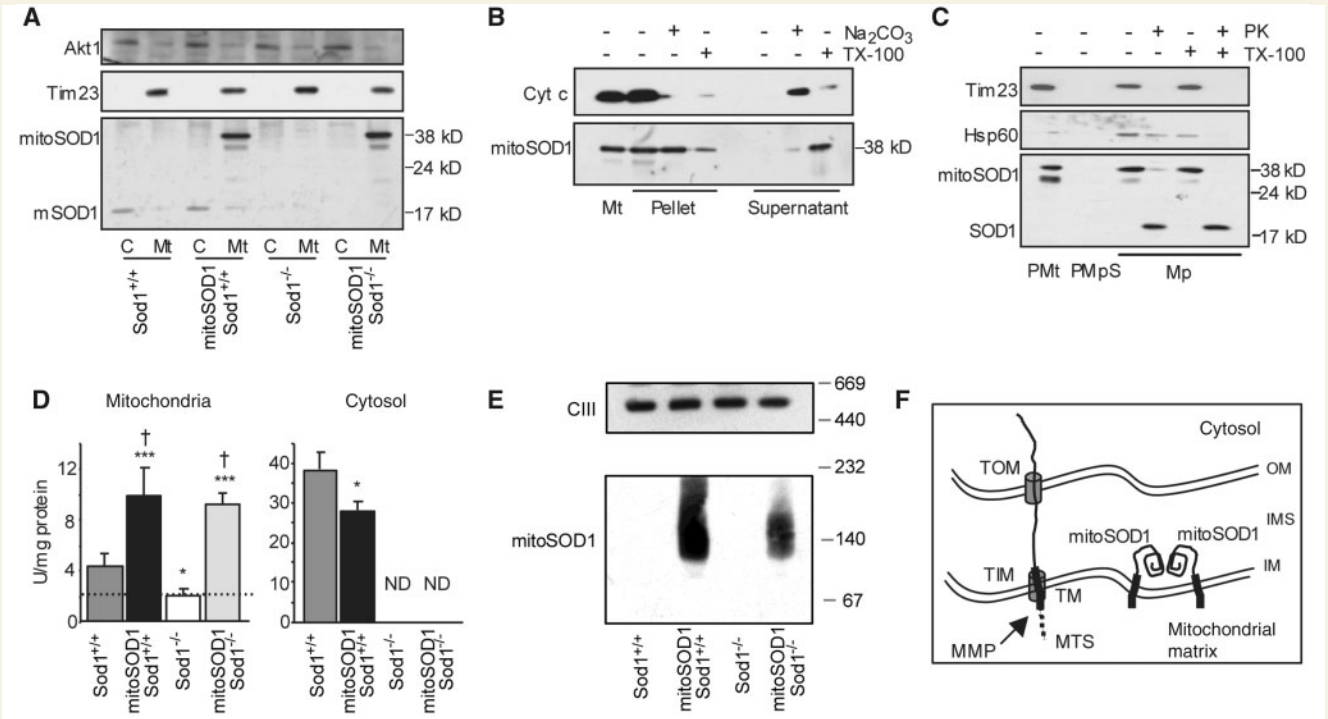

Figure 5 MitoSOD1 localization and enzymatic activity. (**A**) Western blot of spinal cord mitochondria (Mt) and cytosolic fractions (C) demonstrating mitochondrial localization of mitoSOD1. (**B**) Protein alkaline extraction. Western blot of the pellet and supernatant of *mitoSOD1,Sod*$^{+/+}$ brain mitochondria ± Na_2CO_3 or Triton X-100 (TX-100). (**C**) Proteinase K (PK) digestion. Western blot of mitoplasts (Mp) ± proteinase K or TX-100. Mitoplasts were prepared from *mitoSOD1,Sod1*$^{+/+}$ brain purified mitochondria (PMt) treated with digitonin (PMpS, post-mitoplast supernatant). (**D**) KCN-sensitive SOD activity in mitochondrial and cytosolic fractions from spinal cord (*$P < 0.05$ and ***$P < 0.0005$ versus *Sod1*$^{+/+}$, $^{\dagger}P < 0.05$ versus *Sod1*$^{-/-}$; ANOVA with Fisher *post hoc* test; $n = 3$–5 animals per group). The dashed line defines the inhibition of cyt *c* reduction in mitochondria that is not dependent on SOD1. (**E**) Complex III (CIII), detected by an antibody against core II protein, was used as a loading control representative of high molecular weight mitochondrial protein complexes. (**F**) Schematic of the proposed mechanism of mitoSOD1 import and maturation in mitochondria. OM = outer membrane; IM = inner membrane; TOM and TIM = translocators of the outer membrane and inner membrane, respectively; MTS = mitochondrial targeting sequence; MMP = matrix metalloproteinases; TM = transmembrane domain; Tim23 = mitochondrial inner membrane protein; Akt1 = cytosolic soluble protein; cyt *c* = soluble intermembrane space protein; Hsp60 = soluble mitochondrial matrix protein; ND = activity not detectable.

membrane tethering, SOD1 activity was also measured spectrophotometrically in spinal cord cytosol and intact mitochondrial fractions (Fig. 5D). We found 3- and 3.5-fold higher SOD1 activity in *mitoSOD1,Sod1*$^{-/-}$ and *mitoSOD1,Sod1*$^{+/+}$ mitochondria, respectively, compared to *Sod1*$^{+/+}$. Note that these values were obtained after subtraction of non-specific cytochrome *c* reductase activity present in mitochondria (indicated by the dashed line in Fig. 5D). KCN-sensitive SOD activity was undetectable in the cytosolic fraction of *mitoSOD1,Sod1*$^{-/-}$ spinal cord. These data confirm that mitoSOD1 is enzymatically active and that its activity is exclusively localized to mitochondria. We also found a moderate but significant reduction of SOD1 activity in *mitoSOD,Sod1*$^{+/+}$ cytosol, as compared to *Sod1*$^{+/+}$.

Since the active form of SOD1 is predominantly a dimer (Tainer *et al.*, 1982; Hornberg *et al.*, 2007), we looked for mitoSOD1 oligomerization by blue native gel electrophoresis and western blot of spinal cord mitochondria. In this experiment, proteins are maintained in their native state and separated in a non-denaturing gel, which allows the preservation of protein complexes that are detected with specific antibodies. In *mitoSOD1,Sod1*$^{+/+}$ and *mitoSOD1,Sod1*$^{-/-}$ mitochondria, we observed a major band with an estimated size of 100–120 kDa (Fig. 5E) and a smear of higher molecular weight protein complexes, which indicate higher orders of oligomerization than a simple dimer. Since the monomer of mitoSOD1 is 38 kDa, this result suggests that the transgenic protein oligomerizes on the mitochondrial IM. In addition, we observed that mitochondria of *mitoSOD1,Sod1*$^{+/+}$ contained a larger amount of oligomeric SOD1 than *mitoSOD1,Sod1*$^{-/-}$, suggesting that endogenous SOD1 in mitochondria participates to the formation of multiple species of oligomeric complexes.

The proposed scheme for import and maturation of mitoSOD1 in mitochondria is shown in Fig. 5F. We suggest that mitoSOD1 enters the intermembrane space through the translocator of the outer membrane, where the mitochondrial targeting sequence is engaged in the translocator of the inner membrane, exposed to the matrix and cleaved by matrix metalloproteinases. Upon processing, the transmembrane domain allows for the insertion of the protein in the inner membrane with the SOD1 portion facing the intermembrane space. We propose that mitoSOD1 folds and acquires metals in the intermembrane space to reach its mature and enzymatically active state. Active dimers/oligomers of SOD1 may result from the juxtaposition of adjacent mitoSOD1 molecules on the inner membrane.

MitoSOD1 rescues axon outgrowth and mitochondrial defects *in vitro*

Primary motor neurons were cultured from *mitoSOD1,Sod1*$^{-/-}$ mice, and mitochondrial localization of human SOD1 was verified by immunocytochemistry (Fig. 6A). Staining with a monoclonal antibody specific for human SOD1 revealed a punctate distribution. This staining was absent in cells negative for the *mitoSOD1* transgene (not shown). Double labelling with Mitotracker Red CM-H_2XRos revealed precise colocalization of human SOD1 staining with mitochondria.

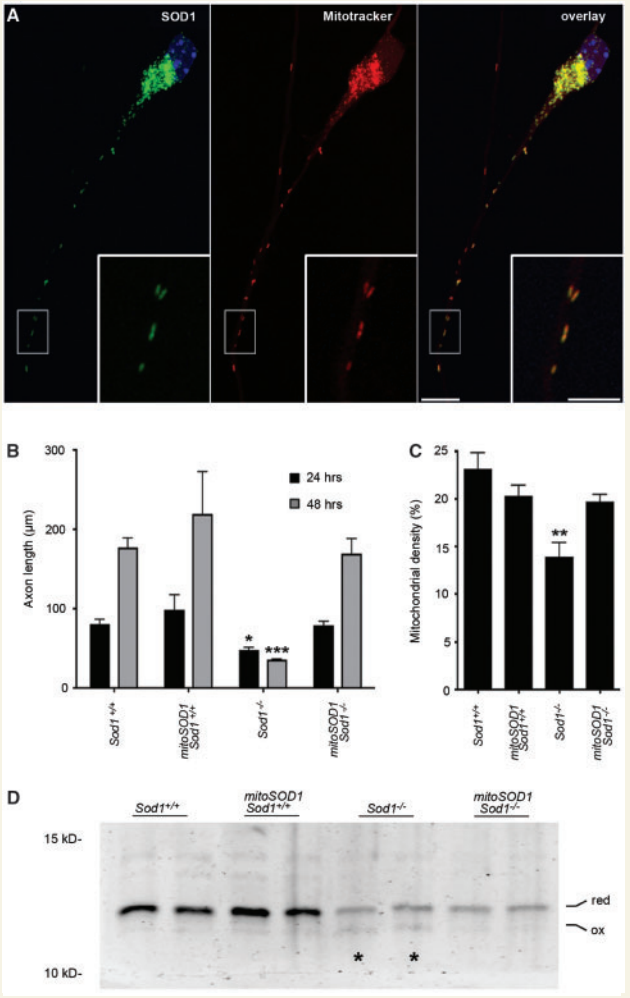

Figure 6 MitoSOD1 rescues axon outgrowth and normalizes mitochondrial density in *Sod1*$^{-/-}$ primary motor neurons. (**A**) Mitochondrial localization of mitoSOD1 was verified by double labelling for human SOD1 (Sigma antibody, in green) and Mitotracker Red CM-H_2XRos. A representative *mitoSOD1,Sod1*$^{-/-}$ motor neuron (24 h) is shown. Scale bar = 10 µm (inset 5 µm). (**B**) Axon length at 24 and 48 h in culture (24 h: $*P < 0.05$, *Sod1*$^{-/-}$ versus all other genotypes; 48 h: $***P < 0.001$, *Sod1*$^{-/-}$ versus all other genotypes; $P > 0.05$ for all other comparisons; ANOVA with Tukey *post hoc* test). (**C**) Mitochondrial density, calculated as the summed length of all mitochondria in the axon, divided by the axon length ($**P < 0.01$, *Sod1*$^{-/-}$ versus all other genotypes; ANOVA with Tukey *post hoc* test). In **B** and **C**, mean ± SEM is shown from multiple motor neuron preparations, needed to generate at least $n = 3$ replicates per genotype. (**D**) Thioredoxin-2 redox western from cortical neurons (72 h in culture). Oxidation of thioredoxin-2 (asterisks) is attenuated in *mitoSOD1,Sod1*$^{-/-}$ neurons. Note that protein loading was not equalized between samples (refer to 'Methods' section).

Axon outgrowth was measured in primary motor neurons at 24 and 48 h (Fig. 6B). MitoSOD1 showed a robust protective effect in *mitoSOD1,Sod1*$^{-/-}$ motor neurons, restoring growth characteristics and axon length to wild-type levels. Axon length

at 24 h (mean ± SEM) in *Sod1*$^{-/-}$ motor neurons was 47 ± 4 μm, compared with 78 ± 6 μm in *mitoSOD1,Sod1*$^{-/-}$ motor neurons ($P < 0.05$). At 48 h, *Sod1*$^{-/-}$ motor axons were 34 ± 2 μm in length, while *mitoSOD1,Sod1*$^{-/-}$ motor axons doubled in length to 169 ± 19 μm ($P < 0.001$). Thus, mitoSOD1 is properly localized to motor neuron mitochondria *in vitro* and rescues *Sod1*$^{-/-}$ axon outgrowth. MitoSOD1 also normalized mitochondrial density in *mitoSOD1,Sod1*$^{-/-}$ motor axons (Fig. 6C), and suppressed thioredoxin-2 oxidation in *mitoSOD1,Sod1*$^{-/-}$ cortical neurons (Fig. 6D).

MitoSOD1 preserves neuromuscular junction integrity and grip strength *in vivo*

Cohorts of *Sod1*$^{-/-}$ and *mitoSOD1,Sod1*$^{-/-}$ mice (and littermate controls) were followed to 12 months of age for assessment of neuromuscular junction innervation and grip strength. Morphological analysis of neuromuscular junction in tibialis anterior muscle showed a robust protective effect of mitoSOD1 at 4, 8 and 12 months of age (Fig. 7A and B). At 4 months, 92.5 ± 0.3% of endplates were fully innervated in *mitoSOD1,Sod1*$^{-/-}$ mice, which were indistinguishable from controls (92.9 ± 1%). As the animals aged to 8 and 12 months, *mitoSOD1 Sod1*$^{-/-}$ neuromuscular junctions remained fully innervated.

Similarly, on grip strength analysis, *mitoSOD1,Sod1*$^{-/-}$ mice performed as well as controls, compared to *Sod1*$^{-/-}$ littermates that showed a significantly reduced latency to fall (Fig. 7C). These data demonstrate that *mitoSOD1* is sufficient to prevent both the pathological and phenotypical hallmarks of motor axonopathy in *Sod1*$^{-/-}$ mice.

Discussion

Altered mitochondrial function and dynamics have emerged as a major cause of axonal degeneration in peripheral neuropathy and motor neuron disease (Baloh, 2008; Magrané and Manfredi, 2009). Here, we investigated how SOD1 expression in the mitochondrial intermembrane space influences motor axon survival. A protective function for SOD1 in the intermembrane space has been suggested by reports of mitochondrial oxidative stress and

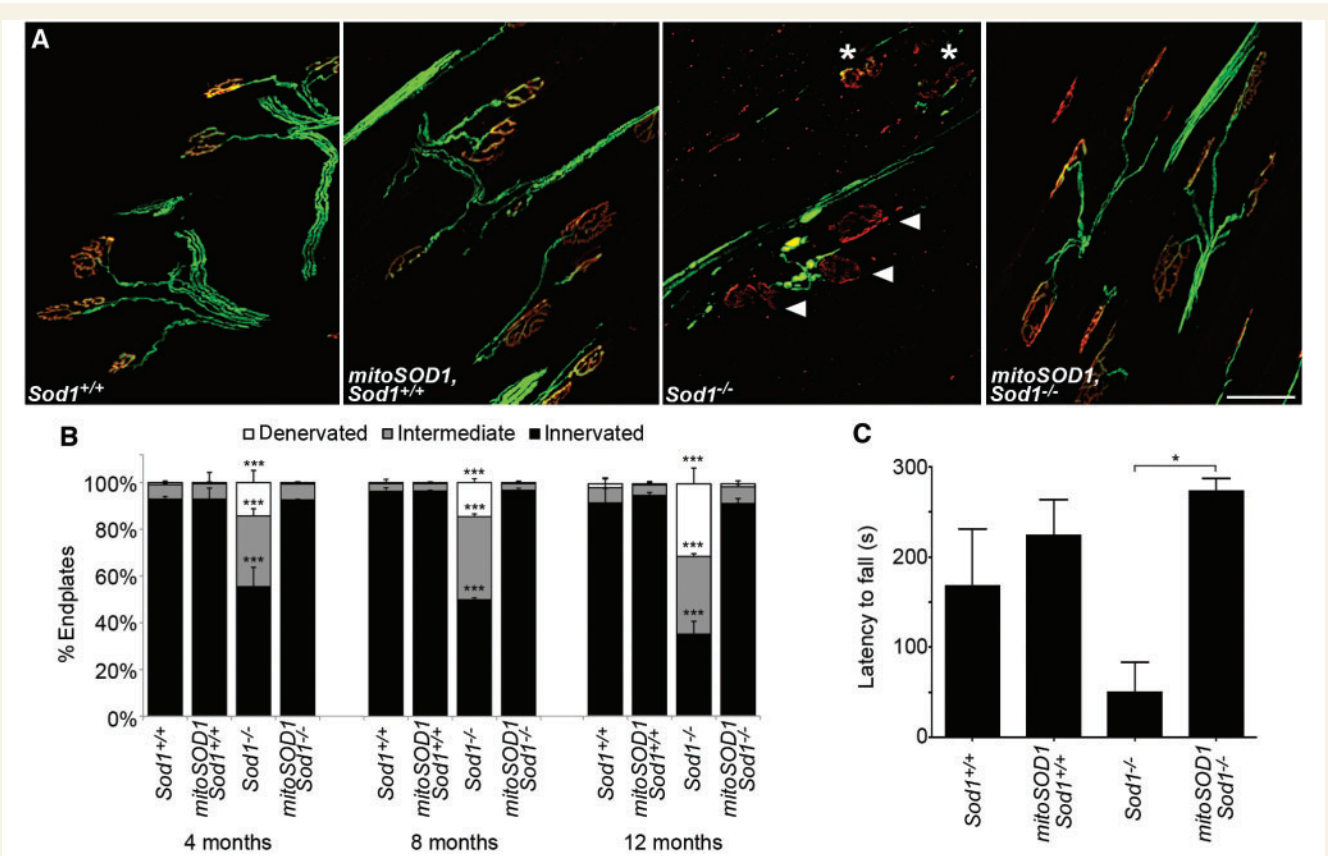

Figure 7 MitoSOD1 prevents denervation at the neuromuscular junction and rescues the *Sod1*$^{-/-}$ phenotype. (**A**) Representative images of neuromuscular junctions from tibialis anterior at 12 months. Numerous intermediate (asterisks) and denervated (arrowheads) endplates are seen in *Sod1*$^{-/-}$ mice, but are rarely observed in control animals or in *mitoSOD1,Sod1*$^{-/-}$ mice (scale bar = 50 μm). (**B**) Quantitative comparison of neuromuscular junction innervation at 4, 8 and 12 months of age. No significant difference was seen between *mitoSOD1,Sod1*$^{-/-}$, *Sod1*$^{+/+}$ and *mitoSOD1,Sod1*$^{+/+}$ mice at any time point. Endplates (964 ± 105) were assessed per muscle (***$P < 0.001$ for *Sod1*$^{-/-}$ versus all other genotypes; ANOVA with Tukey *post hoc* test; $n = 3$ mice per group). (**C**) Latency to fall on grip strength testing at 12 months of age (*$P < 0.05$; ANOVA with Tukey *post hoc* test; $n = 3$–4 per group).

oxidative damage due to deletion of SOD1 (Aquilano *et al.*, 2006; Muller *et al.*, 2007; Jang *et al.*, 2010), although one group reported that SOD1 potentiates mitochondrial reactive oxygen species generation due to respiratory chain inhibition (Goldsteins *et al.*, 2008). None of these studies addressed the functional effect of intermembrane space-localized SOD1 on oxidative stress-mediated pathology.

Mitochondrial superoxide production and intermembrane space SOD1

The protective effect of mitoSOD1 suggests that SOD1 in the intermembrane space is important for regulating physiologic $O_2{\cdot}^-$ levels. The major source of intracellular $O_2{\cdot}^-$ production is the electron transport chain, located along the mitochondrial inner membrane. Complex I releases $O_2{\cdot}^-$ into the mitochondrial matrix (the site of SOD2 expression), and complex III releases $O_2{\cdot}^-$ bidirectionally into the matrix and intermembrane space (Han *et al.*, 2001; Muller *et al.*, 2004). SOD1 may, therefore, play a protective role by neutralizing complex III-derived $O_2{\cdot}^-$ in the intermembrane space. This is supported by our finding of thioredoxin-2 oxidation in the setting of a normal thioredoxin-1 redox potential, and by a previous report of preferential protein oxidation in mitochondria, rather than the cytosol, following SOD1 knockdown (Aquilano *et al.*, 2006).

Our data suggest that loss of SOD1, at least acutely, causes a redox imbalance within mitochondria that is not transmitted to the cytosol. Previous reports of increased mitochondrial reactive oxygen species release in *Sod1*$^{-/-}$ mice and *C. elegans* did not address the question of the cytosolic redox state (Muller *et al.*, 2007; Yanase *et al.*, 2009; Jang *et al.*, 2010). Elchuri and colleagues (2005) measured cytosolic and mitochondrial aconitase activity in *Sod1*$^{-/-}$ mouse liver, and found a significant decrease in the activity of both enzymes with age, suggesting an excess of $O_2{\cdot}^-$ in both compartments. Whether cytosolic aconitase inactivation in liver represents spilling of mitochondrial $O_2{\cdot}^-$ into the cytosol, or excess $O_2{\cdot}^-$ from other typically minor sources, such as cellular oxidases and cytochrome P450s, is unclear.

We cannot exclude the possibility that mitoSOD1 in the intermembrane space may be scavenging $O_2{\cdot}^-$ generated by other sources, such as membrane-associated NADPH oxidase. However, $O_2{\cdot}^-$ is unlikely to diffuse far from its site of production without undergoing reactions to produce other reactive oxygen species. Moreover, negatively charged $O_2{\cdot}^-$ cannot freely diffuse across lipid bilayers (Gus'kova *et al.*, 1984), although it is transmitted by voltage-dependent anion channels (Han *et al.*, 2003), and a small fraction exists in the membrane permeable protonated form ($HO_2{\cdot}$) at neutral pH (Halliwell and Gutteridge, 1990). $O_2{\cdot}^-$ may also spontaneously convert to membrane-permeable H_2O_2 at a rate 4-fold slower than the SOD1-catalysed reaction. However, excess cytosolic H_2O_2 would be detected as thioredoxin-1 oxidation in our assay, since both thioredoxin-1 and thioredoxin-2 are oxidized by H_2O_2 (Hansen *et al.*, 2006b).

The contribution of SOD1 to $O_2{\cdot}^-$ neutralization from other sources could be tested by alternative targeting strategies, taking care to prevent SOD1 from being accessible for mitochondrial import. For example, SOD1 could be tethered to the inner face of the plasma membrane or targeted to the endoplasmic reticulum. Further analysis is also needed to define the compartmental redox changes leading to denervation *in vivo,* although subcellular fractionation analysis of neuromuscular junction contents is not feasible with current techniques. New methods for assessing mitochondrial versus cytosolic redox state at the neuromuscular junction *in vivo* are needed.

This study also raises the question of the relative roles of SOD1 and SOD2 in maintaining the mitochondrial redox state and in motor axon maintenance. Loss of SOD2 in mice causes neonatal lethality associated with CNS and cardiac pathology and extensive mitochondrial damage, demonstrating a vital role in development (Lebovitz *et al.*, 1996). Conditional knockout of SOD2 in adult motor neurons does not cause motor neuron loss, denervation or muscle atrophy up to 9 months of age, although it is associated with accelerated axon degeneration following nerve transection (Misawa *et al.*, 2006). We did not directly address how mitoSOD1 affected SOD2 levels or activity in the current study, but SOD2 activity was previously shown to be unaffected in *Sod1*$^{-/-}$ mice (Muller *et al.*, 2006), and is therefore unlikely to account for our observation of preferential mitochondrial redox changes in this model.

Mitochondrial SOD1 import

Like many other intermembrane space proteins, native SOD1 lacks a canonical mitochondrial targeting sequence. Mitochondrial import of SOD1 depends on the level of copper chaperone for SOD1 in mitochondria, which in turn depends on oxygen levels and import via the Mia40/Erv1 disulphide relay system (Kawamata and Manfredi, 2008; Reddehase *et al.*, 2009). As a consequence, mitochondrial localization of endogenous SOD1 cannot be experimentally manipulated without influencing the mitochondrial localization of other proteins.

An artificial targeting approach was therefore required to express SOD1 exclusively in the intermembrane space. The mitofilin targeting sequence was chosen because it creates an integral membrane protein, anchoring SOD1 to the outer face of the inner mitochondrial membrane. Endogenous SOD1 is normally thought to be soluble in the intermembrane space, and can be released from mitochondria due to spontaneous increases in outer membrane permeability (Li *et al.*, 2006). Subcellular fractionation studies in *mitoSOD1,Sod1*$^{-/-}$ tissues demonstrate that anchoring of mitoSOD1 effectively prevents unwanted release into the cytosol. SOD1 activity assays in isolated (intact) mitochondria also verify that mitoSOD1 is enzymatically active; therefore, tethering SOD1 to the inner membrane does not abolish its activity. Moreover, native gel electrophoresis demonstrates that mitoSOD1 is capable of oligomerization. Whether this accounts for measured SOD1 activity remains to be seen, but is not strictly required, as isolated SOD1 monomers retain ~10% activity compared to SOD1 dimers (Bertini *et al.*, 1994).

The expression of mitoSOD1 in *mitoSOD1,Sod1*$^{+/+}$ spinal cord results in a modest but significant decrease of cytosolic SOD1 activity as compared to *Sod1*$^{+/+}$ mice (Fig. 5D). The cause for this reduction is unknown, but one hypothesis is that the increased

amount of SOD1 localized in the intermembrane space may decrease the amounts of copper or copper chaperone for SOD1 available for the maturation and function of endogenous SOD1 in the cytosol (Kawamata and Manfredi, 2008). This change was insufficient to cause a phenotypic change in *MitoSOD1,Sod1*$^{+/+}$ mice, which was indistinguishable from wild-type controls in multiple assays.

Mitochondrial defects and motor axonopathy

The spatiotemporal sequence of motor pathology has been investigated in numerous mouse models of motor neuron disease, including mutant SOD1-mediated familial amyotrophic lateral sclerosis (Fischer *et al.*, 2004; Pun *et al.*, 2006), spinal muscular atrophy (Murray *et al.*, 2008), progressive motoneuropathy (Holtmann *et al.*, 1999) and others (reviewed in Fischer and Glass, 2007). Distal axonal degeneration, or 'dying-back' at the neuromuscular junction is an early pathological feature in these models and appears to correlate most closely with disease progression. Here, we report progressive denervation in *Sod1*$^{-/-}$ mice reminiscent of these traditional models of motor neuron disease, occurring in the setting of chronic oxidative stress.

Maintenance of extensive axonal processes relies on proper trafficking and function of mitochondria. For example, mutations in *MFN2* and *GDAP1*, regulators of mitochondrial fission and fusion, cause peripheral neuropathy in Charcot–Marie–Tooth disease (Niemann *et al.*, 2005; Baloh *et al.*, 2007). In *Drosophila,* inactivation of dMiro, a cargo adaptor for anterograde mitochondrial transport, causes accumulation of mitochondria in motor neuron cell bodies and depletion in axons, leading to morphological abnormalities at the neuromuscular junction (Guo *et al.*, 2005). Exposure to the mitochondrial toxin, rotenone (a complex I inhibitor), has also been shown to cause axonal degeneration *in vitro* (Press and Milbrandt, 2008).

Growing evidence suggests that aberrant mitochondrial trafficking and mitochondrial dysfunction promote distal axonal degeneration in motor neuron disease, although the pathogenic mechanism(s) are less clear. Biochemical and structural defects in mitochondria are well described in mutant SOD1 models of familial amyotrophic lateral sclerosis (Kong and Xu, 1998; Mattiazzi *et al.*, 2002; Menzies *et al.*, 2002), in which mutant SOD1 accumulates and forms insoluble aggregates in mitochondria (Liu *et al.*, 2004). Alterations in axonal transport of mitochondria are also seen in mutant SOD1 models, and abnormal mitochondrial clustering and a relative depletion of mitochondria in axons have been reported (De Vos *et al.*, 2007; Magrané *et al.*, 2009; Sotelo-Silveira *et al.*, 2009). This parallels anecdotal observations from human amyotrophic lateral sclerosis showing abnormal mitochondrial clustering and mitochondrial accumulation in proximal axons and cell bodies of motor neurons (Sasaki and Iwata, 2007). Primary culture models of spinal muscular atrophy demonstrate diminished ATP production, mitochondrial depolarization and reduced mitochondrial density in axons (Acsadi *et al.*, 2009; Wen *et al.*, 2010). Similar findings have also been reported in models of spinal and bulbar muscular atrophy (Piccioni *et al.*, 2002; Ranganathan *et al.*, 2009). Thus despite having different upstream causes, mitochondrial pathology appears to lie along a final common pathway of motor axon degeneration.

In the current study, we report a 40% decrease in mitochondrial density in *Sod1*$^{-/-}$ axons, preventable by introduction of mitoSOD1. We utilized a dye that accumulates in polarized mitochondria, and therefore we cannot exclude that mitochondria were still present in *Sod1*$^{-/-}$ axons in the depolarized state. Further investigation is needed to determine the link between oxidative stress and altered mitochondrial trafficking in this model, and to investigate whether mitochondria are depleted in motor axon terminals prior to denervation *in vivo.* Importantly, we demonstrate that mitochondrial-targeted intervention in this model is sufficient to restore the density of polarized mitochondria in axons and to prevent denervation *in vivo.* It is unclear if mitoSOD1 would be protective in other models of motor neuropathy, where endogenous SOD1 expression is normal, although may be beneficial in models with a strong oxidative stress component.

Conclusion

Targeted replacement of SOD1 in the mitochondrial intermembrane space is sufficient for robust protection against motor axonopathy and mitochondrial abnormalities in *Sod1*$^{-/-}$ motor neurons. This suggests that mitochondrial damage is an underlying cause of distal motor axonopathy in *Sod1*$^{-/-}$ mice. Moreover, the functional requirement for SOD1 in motor axons may be based on a protective role in mitochondria.

Acknowledgements

We thank Marie Csete for providing *Sod1*$^{-/-}$ breeders, Seneshaw Asress for technical assistance and Wilfried Rossoll and Fang Wu for instruction on primary cultures.

Funding

Robert Packard Centre for ALS Research (to G.M. and J.G.); and the National Institutes of Health (grant numbers T32-ES12870 to L.F., R01-NS051419 to G.M. and R01-NS062055 to G.M.).

Supplementary material

Supplementary material is available at *Brain* online.

References

Acin-Perez R, Salazar E, Kamenetsky M, Buck J, Levin LR, Manfredi G. Cyclic AMP produced inside mitochondria regulates oxidative phosphorylation. Cell Metab 2009; 9: 265–76.

Acsadi G, Lee I, Li X, Khaidakov M, Pecinova A, Parker GC, et al. Mitochondrial dysfunction in a neural cell model of spinal muscular atrophy. J Neurosci Res 2009; 87: 2748–56.

Aquilano K, Vigilanza P, Rotilio G, Ciriolo MR. Mitochondrial damage due to SOD1 deficiency in SH-SY5Y neuroblastoma cells: a rationale for the redundancy of SOD1. FASEB J 2006; 20: 1683–5.

Arnér ES, Holmgren A. Physiological functions of thioredoxin and thioredoxin reductase. Eur J Biochem 2000; 267: 6102–9.

Azzi A, Montecucco C, Richter C. The use of acetylated ferricytochrome c for the detection of superoxide radicals produced in biological membranes. Biochem Biophys Res Commun 1975; 65: 597–603.

Baloh RH. Mitochondrial dynamics and peripheral neuropathy. The Neuroscientist 2008; 14: 12–8.

Baloh RH, Schmidt RE, Pestronk A, Milbrandt J. Altered axonal mitochondrial transport in the pathogenesis of Charcot-Marie-Tooth disease from mitofusin 2 mutations. J Neurosci 2007; 27: 422–30.

Bertini I, Piccioli M, Viezzoli MS, Chiu CY, Mullenbach GT. A spectroscopic characterization of a monomeric analog of copper, zinc superoxide dismutase. Eur Biophys J 1994; 23: 167–76.

Bjornskov EK, Norris FH, Mower-Kuby J. Quantitative axon terminal and end-plate morphology in amyotrophic lateral sclerosis. Arch Neurol 1984; 41: 527–30.

Borchelt DR, Davis J, Fischer M, Lee MK, Slunt HH, Ratovitsky T, et al. A vector for expressing foreign genes in the brains and hearts of transgenic mice. Genet Anal 1996; 13: 159–63.

De Vos KJ, Chapman AL, Tennant ME, Manser C, Tudor EL, Lau KF, et al. Familial amyotrophic lateral sclerosis-linked SOD1 mutants perturb fast axonal transport to reduce axonal mitochondria content. Hum Mol Genet 2007; 16: 2720–8.

Elchuri S, Oberley TD, Qi W, Eisenstein RS, Jackson Roberts L, Van Remmen H, et al. CuZnSOD deficiency leads to persistent and widespread oxidative damage and hepatocarcinogenesis later in life. Oncogene 2005; 24: 367–80.

Feng G, Mellor RH, Bernstein M, Keller-Peck C, Nguyen QT, Wallace M, et al. Imaging neuronal subsets in transgenic mice expressing multiple spectral variants of GFP. Neuron 2000; 28: 41–51.

Fischer LR, Culver D, Tennant P, Davis A, Wang M, Castellano-Sanchez A, et al. Amyotrophic lateral sclerosis is a distal axonopathy: evidence in mice and man. Exp Neurol 2004; 185: 232–40.

Fischer LR, Glass J. Axonal degeneration in motor neuron disease. Neurodegener Dis 2007; 4: 431–42.

Flood DG, Reaume AG, Gruner JA, Hoffman EK, Hirsch JD, Lin YG, et al. Hindlimb motor neurons require Cu/Zn superoxide dismutase for maintenance of neuromuscular junctions. Am J Pathol 1999; 155: 663–72.

Goldsteins G, Keksa-Goldsteine V, Ahtoniemi T, Jaronen M, Arens E, Akerman K, et al. Deleterious role of superoxide dismutase in the mitochondrial intermembrane space. J Biol Chem 2008; 283: 8446–52.

Gould TW, Buss RR, Vinsant S, Prevette D, Sun W, Knudson CM, et al. Complete dissociation of motor neuron death from motor dysfunction by Bax deletion in a mouse model of ALS. J Neurosci 2006; 26: 8774–86.

Guo X, Macleod G, Wellington A, Hu F, Panchumarthi S, Schoenfield M, et al. The GTPase dMiro is required for axonal transport of mitochondria to synapses. Neuron 2005; 47: 379–93.

Gus'kova RA, Ivanov II, Kol'tover VK, Akhobadze VV, Rubin AB. Permeability of bilayer lipid membranes for superoxide (O2-.) radicals. Biochim Biophys Acta 1984; 778: 579–85.

Halliwell B, Gutteridge JM. Role of free radicals and catalytic metal ions in human disease: an overview. Meth Enzymol 1990; 186: 1–85.

Halvey PJ, Watson WH, Hansen JM, Go YM, Samali A, Jones DP. Compartmental oxidation of thiol-disulphide redox couples during epidermal growth factor signalling. Biochem J 2005; 386: 215–9.

Han D, Antunes F, Canali R, Rettori D, Cadenas E. Voltage-dependent anion channels control the release of the superoxide anion from mitochondria to cytosol. J Biol Chem 2003; 278: 5557–63.

Han D, Williams E, Cadenas E. Mitochondrial respiratory chain-dependent generation of superoxide anion and its release into the intermembrane space. Biochem J 2001; 353 (Pt 2): 411–6.

Hansen J, Zhang H, Jones D. Differential oxidation of thioredoxin-1, thioredoxin-2, and glutathione by metal ions. Free Radic Biol Med 2006a; 40: 138–45.

Hansen J, Zhang H, Jones D. Mitochondrial thioredoxin-2 has a key role in determining tumor necrosis factor-alpha-induced reactive oxygen species generation, NF-kappaB activation, and apoptosis. Toxicol Sci 2006b; 91: 643–50.

Holtmann B, Zielasek J, Toyka KV, Sendtner M. Comparative analysis of motoneuron loss and functional deficits in PMN mice: implications for human motoneuron disease. J Neurol Sci 1999; 169 (1–2): 140–7.

Hornberg A, Logan DT, Marklund SL, Oliveberg M. The coupling between disulphide status, metallation and dimer interface strength in Cu/Zn superoxide dismutase. J Mol Biol 2007; 365: 333–42.

Huang TT, Yasunami M, Carlson EJ, Gillespie AM, Reaume AG, Hoffman EK, et al. Superoxide-mediated cytotoxicity in superoxide dismutase-deficient fetal fibroblasts. Arch Biochem Biophys 1997; 344: 424–32.

Iñarrea P. Purification and determination of activity of mitochondrial cyanide-sensitive superoxide dismutase in rat tissue extract. Meth Enzymol 2002; 349: 106–14.

Jang YC, Lustgarten MS, Liu Y, Muller FL, Bhattacharya A, Liang H, et al. Increased superoxide in vivo accelerates age-associated muscle atrophy through mitochondrial dysfunction and neuromuscular junction degeneration. FASEB J 2010; 24: 1376–90.

John GB, Shang Y, Li L, Renken C, Mannella CA, Selker JM, et al. The mitochondrial inner membrane protein mitofilin controls cristae morphology. Mol Biol Cell 2005; 16: 1543–54.

Kawamata H, Manfredi G. Different regulation of wild-type and mutant Cu,Zn superoxide dismutase localization in mammalian mitochondria. Hum Mol Genet 2008; 17: 3303–17.

Kong J, Xu Z. Massive mitochondrial degeneration in motor neurons triggers the onset of amyotrophic lateral sclerosis in mice expressing a mutant SOD1. J Neurosci 1998; 18: 3241–50.

Kuthan H, Haussmann HJ, Werringloer J. A spectrophotometric assay for superoxide dismutase activities in crude tissue fractions. Biochem J 1986; 237: 175–80.

Lebovitz R, Zhang H, Vogel H, Cartwright J, Dionne L, Lu N, et al. Neurodegeneration, myocardial injury, and perinatal death in mitochondrial superoxide dismutase-deficient mice. Proc Natl Acad Sci USA 1996; 93: 9782–7.

Li Q, Sato EF, Kira Y, Nishikawa M, Utsumi K, Inoue M. A possible cooperation of SOD1 and cytochrome c in mitochondria-dependent apoptosis. Free Radic Biol Med 2006; 40: 173–81.

Liu J, Lillo C, Jonsson PA, Vande Velde C, Ward CM, Miller TM, et al. Toxicity of familial ALS-linked SOD1 mutants from selective recruitment to spinal mitochondria. Neuron 2004; 43: 5–17.

Magrané J, Hervias I, Henning M, Damiano M, Kawamata H, Manfredi G. Mutant SOD1 in neuronal mitochondria causes toxicity and mitochondrial dynamics abnormalities. Hum Mol Genet 2009; 18: 4552–64.

Magrané J, Manfredi G. Mitochondrial function, morphology, and axonal transport in amyotrophic lateral sclerosis. Antioxid Redox Signal 2009; 11: 1615–26.

Maselli RA, Wollman RL, Leung C, Distad B, Palombi S, Richman DP, et al. Neuromuscular transmission in amyotrophic lateral sclerosis. Muscle Nerve 1993; 16: 1193–203.

Mattiazzi M, D'Aurelio M, Gajewski CD, Martushova K, Kiaei M, Beal MF, et al. Mutated human SOD1 causes dysfunction of oxidative phosphorylation in mitochondria of transgenic mice. J Biol Chem 2002; 277: 29626–33.

McCord JM, Fridovich I. Superoxide dismutase. An enzymic function for erythrocuprein (hemocuprein). J Biol Chem 1969; 244: 6049–55.

Menzies FM, Cookson MR, Taylor RW, Turnbull DM, Chrzanowska-Lightowlers ZM, Dong L, et al. Mitochondrial dysfunction in a cell culture model of familial amyotrophic lateral sclerosis. Brain 2002; 125: 1522–33.

Misawa H, Nakata K, Matsuura J, Moriwaki Y, Kawashima K, Shimizu T, et al. Conditional knockout of Mn superoxide dismutase in postnatal motor neurons reveals resistance to mitochondrial generated superoxide radicals. Neurobiol Dis 2006; 23: 169–77.

Muller F, Song W, Jang Y, Liu Y, Sabia M, Richardson A, et al. Denervation-induced skeletal muscle atrophy is associated with increased mitochondrial ROS production. Am J Physiol Regul Integr Comp Physiol 2007; 293: R1159–68.

Muller F, Song W, Liu Y, Chaudhuri A, Piekedahl S, Strong R, et al. Absence of CuZn superoxide dismutase leads to elevated oxidative stress and acceleration of age-dependent skeletal muscle atrophy. Free Radic Biol Med 2006; 40: 1993–2004.

Muller FL, Liu Y, Van Remmen H. Complex III releases superoxide to both sides of the inner mitochondrial membrane. J Biol Chem 2004; 279: 49064–73.

Murray LM, Comley LH, Thomson D, Parkinson N, Talbot K, Gillingwater T. Selective vulnerability of motor neurons and dissociation of pre- and post-synaptic pathology at the neuromuscular junction in mouse models of spinal muscular atrophy. Hum Mol Genet 2008; 17: 949–62.

Niemann A, Ruegg M, La Padula V, Schenone A, Suter U. Ganglioside-induced differentiation associated protein 1 is a regulator of the mitochondrial network: new implications for Charcot-Marie-Tooth disease. J Cell Biol 2005; 170: 1067–78.

Piccioni F, Pinton P, Simeoni S, Pozzi P, Fascio U, Vismara G, et al. Androgen receptor with elongated polyglutamine tract forms aggregates that alter axonal trafficking and mitochondrial distribution in motor neuronal processes. FASEB J 2002; 16: 1418–20.

Press C, Milbrandt J. Nmnat delays axonal degeneration caused by mitochondrial and oxidative stress. J Neurosci 2008; 28: 4861–71.

Pun S, Santos AF, Saxena S, Xu L, Caroni P. Selective vulnerability and pruning of phasic motoneuron axons in motoneuron disease alleviated by CNTF. Nat Neurosci 2006; 9: 408–19.

Ranganathan S, Harmison GG, Meyertholen K, Pennuto M, Burnett BG, Fischbeck KH. Mitochondrial abnormalities in spinal and bulbar muscular atrophy. Human Mol Genet 2009; 18: 27–42.

Reaume AG, Elliott JL, Hoffman EK, Kowall NW, Ferrante RJ, Siwek DF, et al. Motor neurons in Cu/Zn superoxide dismutase-deficient mice develop normally but exhibit enhanced cell death after axonal injury. Nat Genet 1996; 13: 43–7.

Reddehase S, Grumbt B, Neupert W, Hell K. The disulfide relay system of mitochondria is required for the biogenesis of mitochondrial Ccs1 and Sod1. J Mol Biol 2009; 385: 331–8.

Rouaux C, Panteleeva I, René F, Gonzalez De Aguilar J-L, Echaniz-Laguna A, Dupuis L, et al. Sodium valproate exerts neuroprotective effects in vivo through CREB-binding protein-dependent mechanisms but does not improve survival in an amyotrophic lateral sclerosis mouse model. J Neurosci 2007; 27: 5535–45.

Sasaki S, Iwata M. Mitochondrial alterations in the spinal cord of patients with sporadic amyotrophic lateral sclerosis. J Neuropathol Exp Neurol 2007; 66: 10–6.

Schagger H, von Jagow G. Blue native electrophoresis for isolation of membrane protein complexes in enzymatically active form. Anal Biochem 1991; 199: 223–31.

Shefner JM, Reaume AG, Flood DG, Scott RW, Kowall NW, Ferrante RJ, et al. Mice lacking cytosolic copper/zinc superoxide dismutase display a distinctive motor axonopathy. Neurology 1999; 53: 1239–46.

Sotelo-Silveira JR, Lepanto P, Elizondo MV, Horjales S, Palacios F, Martinez Palma L, et al. Axonal mitochondrial clusters containing mutant SOD1 in transgenic models of ALS. Antioxid Redox Signal 2009; 11: 1–11.

Sturtz LA, Diekert K, Jensen LT, Lill R, Culotta VC. A fraction of yeast Cu,Zn-superoxide dismutase and its metallochaperone, CCS, localize to the intermembrane space of mitochondria. A physiological role for SOD1 in guarding against mitochondrial oxidative damage. J Biol Chem 2001; 276: 38084–9.

Suzuki M, McHugh J, Tork C, Shelley B, Klein SM, Aebischer P, et al. GDNF secreting human neural progenitor cells protect dying motor neurons, but not their projection to muscle, in a rat model of familial ALS. PLoS ONE 2007; 2: e689.

Tainer JA, Getzoff ED, Beem KM, Richardson JS, Richardson DC. Determination and analysis of the 2 A-structure of copper, zinc superoxide dismutase. J Mol Biol 1982; 160: 181–217.

Vijayvergiya C, Beal MF, Buck J, Manfredi G. Mutant superoxide dismutase 1 forms aggregates in the brain mitochondrial matrix of amyotrophic lateral sclerosis mice. J Neurosci 2005; 25: 2463–70.

Vives-Bauza C, Starkov A, Garcia-Arumi E. Measurements of the antioxidant enzyme activities of superoxide dismutase, catalase, and glutathione peroxidase. Methods Cell Biol 2007; 80: 379–93.

Wang J, Xu G, Slunt H, Gonzales V, Coonfield M, Fromholt D, et al. Coincident thresholds of mutant protein for paralytic disease and protein aggregation caused by restrictively expressed superoxide dismutase cDNA. Neurobiol Dis 2005; 20: 943–52.

Weisiger RA, Fridovich I. Mitochondrial superoxide dismutase. Site of synthesis and intramitochondrial localization. J Biol Chem 1973; 248: 4793–6.

Wen H-L, Lin Y-T, Ting C-H, Lin-Chao S, Li H, Hsieh-Li HM. Stathmin, a microtubule-destabilizing protein, is dysregulated in spinal muscular atrophy. Human Mol Genet 2010; 19: 1766–78.

Yanase S, Onodera A, Tedesco P, Johnson TE, Ishii N. SOD-1 deletions in Caenorhabditis elegans alter the localization of intracellular reactive oxygen species and show molecular compensation. J Gerontol A Biol Sci Med Sci 2009; 64: 530–9.

Zelko IN, Mariani TJ, Folz RJ. Superoxide dismutase multigene family: a comparison of the CuZn-SOD (SOD1), Mn-SOD (SOD2), and EC-SOD (SOD3) gene structures, evolution, and expression. Free Radic Biol Med 2002; 33: 337–49.

Zhang H, Xing L, Rossoll W, Wichterle H, Singer RH, Bassell GJ. Multiprotein complexes of the survival of motor neuron protein SMN with Gemins traffic to neuronal processes and growth cones of motor neurons. J Neurosci 2006; 26: 8622–32.